

# 1 Asymmetric hysteresis loops and smearing of the dielectric anomaly 2 at the transition temperature due to space charges in ferroelectric thin films

3 I. B. Misirlioglu,<sup>1,a)</sup> M. B. Okatan,<sup>2</sup> and S. P. Alpay<sup>2,3</sup>

4 <sup>1</sup>Faculty of Engineering and Natural Sciences, Sabanci University, Tuzla-Orhanli, 34956 Istanbul, Turkey

5 <sup>2</sup>Department of Chemical, Materials, and Biomolecular Engineering, Materials Science  
6 and Engineering Program, and Institute of Materials Science, University of Connecticut,  
7 Storrs, Connecticut 06269, USA

8 <sup>3</sup>Department of Physics, University of Connecticut, Storrs, Connecticut 06269, USA

9 (Received 16 April 2010; accepted 29 May 2010; published online xx xx xxxx)

10 Ferroelectric thin films often exhibit a displacement of the polarization versus the electric field  
11 hysteresis loops, particularly along the electric field axis. This shift is typically attributed to  
12 structural and electronic asymmetry of the film-electrode interfaces, asymmetric surface fields, as  
13 well as space charge regions. In this study, we analyze the effect of a spatial, continuous distribution  
14 of space charge on the hysteresis response and phase transition characteristics of epitaxial (001)  
15 PbZr<sub>0.3</sub>Ti<sub>0.7</sub>O<sub>3</sub> thin films sandwiched between metallic electrodes on (001) SrTiO<sub>3</sub> substrate. Using  
16 a nonlinear thermodynamic model, we compute numerically the internal electrical fields and  
17 polarizations for several different space charge distributions both in the presence of a triangular  
18 external electric field and as a function of temperature at zero applied field. We show that space  
19 charge accumulated near the metal-ferroelectric interfaces can dramatically displace the hysteresis  
20 along the electric field axis such that the otherwise symmetric coercive fields  $E_{C-}$  and  $E_{C+}$  in a bulk  
21 ferroelectric related to each other through  $|E_{C-}|=E_{C+}$  may shift depending on the space charge  
22 concentration in such a manner that both  $E_{C-}, E_{C+} > 0$  or  $E_{C-}, E_{C+} < 0$ . This gives rise to a very  
23 strong imprint. Our findings reveal that the presence of space charges in ferroelectric thin films  
24 results in significant changes in the phase transition characteristics, including a reduction in the  
25 phase transition temperature, smearing of the transition over a temperature range instead of a sharp  
26 dielectric anomaly at the bulk Curie temperature, and a reduction in the dielectric response  
27 compared to defect-free ferroelectrics of the same composition. © 2010 American Institute of  
28 Physics. [doi:10.1063/1.3457348]

## 30 I. INTRODUCTION

31 All physical properties of ferroelectrics (FEs) are very  
32 sensitive to the presence of defects (vacancies, dislocations,  
33 impurities, etc.) and their concentration as these can alter the  
34 local dipole order due to the coupling of their eigenstrains  
35 and/or electrostatic fields with the polarization.<sup>1-3</sup> These ma-  
36 terials are also wide band-gap semiconductors that produce  
37 Schottky-type interfaces when brought in contact with me-  
38 tallic electrodes.<sup>4-8</sup> Such effects become more pronounced in  
39 thin films and multilayers of FEs where imperfections such  
40 as oxygen vacancies inevitably form due to processing  
41 conditions<sup>9,10</sup> and linear defects such as misfit and threading  
42 dislocation may be generated because of the lattice misfit.<sup>11</sup>  
43 A number of studies have focused on the analysis of space  
44 charges in films and superlattices to distinguish the possible  
45 trapped charge contributions from real FE behavior of the  
46 samples.<sup>11-14</sup> The combination of the extrinsic factors such  
47 as trapped charges, concentration variations, and defects with  
48 local strain fields could reduce the polarization stability and  
49 the dielectric response.<sup>2,3,15,16</sup>

AQ: #1 50 An important degradation mechanisms often observed in  
51 FEs is imprint. The most common characteristic of imprint is  
52 the displacement of the polarization versus the applied elec-

tric field hysteresis loop along the electric field axis. This 53  
gives rise to an asymmetry in the remnant polarization and 54  
also an effective variation in the coercive field defined by an 55  
off-set,  $\Delta E = E_{C+} - E_{C-}$ , where  $E_{C+}$  and  $E_{C-}$  are the coercive 56  
fields on the right and left side of the hysteresis loop, respec- 57  
tively. Imprint could result from elevated temperatures due to 58  
asymmetric migration of species along the film, exposure to 59  
UV light or x-rays<sup>17</sup> as well as asymmetric film-electrode top 60  
and bottom interfaces.<sup>18</sup> While the exact mechanisms of im- 61  
print are not known, there is strong experimental evidence 62  
that it results from trapped charges, charged defects, and 63  
other possible defect dipole complexes, surface fields, and 64  
stress gradients. 65

Deposition conditions of thin film materials are often far 66  
from ideal and hence kinetic factors play an important role in 67  
the ultimate stoichiometry of the film.<sup>18-21</sup> As perovskite FEs 68  
have a mix of ionic and covalent interatomic bonding, local 69  
deviations from the exact stoichiometry can create frozen 70  
dipoles and electrostatic fields emanating from these com- 71  
plexes. Furthermore, it has often been discussed that these 72  
“defects” can then trap carriers and become *p*- or *n*-type 73  
centers.<sup>5-8,22</sup> For instance, the surfaces of FE thin films are 74  
highly susceptible to creation of oxygen vacancies during 75  
processing and an electrode-FE film interface is often 76  
thought to be forming a Schottky contact and a commensu- 77  
rate depletion layer. While the effect of the internal electric 78

<sup>a)</sup>Electronic mail: birc@sabanciuniv.edu.

79 fields due to surfaces, structural variations, and trapped  
80 charges, and other defect microstructures on the properties of  
81 FEs is well-understood, theoretical studies of the imprint  
82 phenomenon have focused on charge injection and frozen  
83 average electrostatic fields.<sup>3,6,7,10,23–30</sup>

84 In a recent study, we have shown that internal voltage  
85 off-sets and imprint can result from asymmetrically distrib-  
86 uted trapped space charges described through a constant pla-  
87 nar space charge density in a simple FE capacitor structure  
88 using a nonlinear thermodynamic analysis coupled with  
89 electrostatics.<sup>31</sup> The electrostatic interactions are established  
90 through the built-in polarization due to the space charges and  
91 the spontaneous polarization. Although this simple approach  
92 wherein a monolithic FE is assumed to be composed of “sec-  
93 tions” (or “layers”) with different polarization values when a  
94 constant space charge is discretely inserted at a given posi-  
95 tion within the FE is able to explain the displacement of the  
96 FE hysteresis loops, it can be improved significantly if the  
97 limitations on the position and density of the space charges  
98 are removed. This is the topic of the current work in which  
99 we analyze FE films sandwiched between metallic electrodes  
100 and introduce position-dependent, continuous distribution of  
101 space charge along the thickness of the film. These charges  
102 are thought as fixed-field defects and are distributed inside  
103 the film as a function of position. Our findings reveal that the  
104 hysteresis characteristics of FE films can be altered dramati-  
105 cally under asymmetric spatial variations in the space charge  
106 density. For example, space charges asymmetrically accumu-  
107 lated near the electrode-film interfaces as low as  
108  $0.075 \text{ C/m}^2$  can shift the entire hysteresis loop such that  
109  $E_{C-}, E_{C+} > 0$  or  $E_{C-}, E_{C+} < 0$  compared to an “ideal” FE with  
110  $|E_{C-}| = E_{C+}$  and  $\Delta E = E_{C+} - |E_{C-}| = 0$ . It is also shown that  
111 space charges in FE thin films result in variation in the FE-  
112 paraelectric phase transition (PT) behavior, resulting in a re-  
113 duction in the transition temperature and a smearing of the  
114 transition over a temperature range instead of the sharp di-  
115 electric anomaly at the bulk Curie temperature compared to  
116 defect-free “ideal” FEs of the same composition.

## 117 II. THEORY AND METHODOLOGY

118 Before we proceed with the thermodynamics of a FE  
119 film with an arbitrary volumetric variation in space charges,  
120 we first focus on the distribution of these in vacuum between  
121 two planar electrodes and their potential. We form a one-  
122 dimensional system where there could either be a discrete or  
123 a continuous distribution of charges. The system analyzed  
124 here has its boundaries along the  $z$ -axis and is infinite along  
125 other directions. A simple sandwich-type capacitor structure  
126 with a sheet charge situated at a point  $k$  will have an internal  
127 potential at a point  $j$  given by

$$128 \quad \phi_{j,k} = \frac{\rho A z_j (L - z_k)}{\epsilon_0 L} \quad \text{for } 0 \leq z_j < z_k, \quad (1)$$

$$129 \quad \phi_{j,k} = \frac{\rho A z_k (L - z_j)}{\epsilon_0 L} \quad \text{for } z_k < z_j \leq L, \quad (2)$$

130 which correspond to the analytical solutions of the Poisson’s  
131 equation at all other points other than the charge location

when the electrodes are kept at zero potential. In Eqs. (1) and  
(2),  $\rho$  is the charge density,  $A$  is the area of the capacitor,  $L$  is  
the distance between the electrodes, and  $\epsilon_0$  is the permittivity  
of free space. The indices serve to distinguish the position of  
the sheet charge and its potential at a given location such that  
 $\phi_{j,k}$  stands for the potential at  $j$  due to a charge density  
situated at a point  $k$ . For example, it is clear that there will be  
two different fields in  $+z$  and  $-z$  whose magnitudes are equal  
(but of opposite sign) when the sheet charge is in the middle  
of the capacitor. We note that in the presence of a material  
between the electrodes,  $\epsilon_0$  should be replaced with  $\epsilon_r \cdot \epsilon_0$   
where  $\epsilon_r$  is the background dielectric constant that is basi-  
cally a measure of electronic polarizability of the ions. For a  
sheet of charge  $\rho$  fixed in the center, the fields pointing along  
 $+z$  and  $-z$  will be  $\pm \rho/2\epsilon_0$  when there is no material and  
 $\pm \rho/2\epsilon_0\epsilon_r$  in the presence of a dielectric. For this study,  $\epsilon_r$  is  
taken as ten, corresponding to an optical frequency refractive  
index of  $\sim 3.16$ .<sup>32</sup>

In a periodic or random distribution of space charge,  
there can be a bias field along either  $+z$  or  $-z$  directions  
depending on the charge density as a function of position.  
We assign each discrete point  $k$  a planar charge density that  
is infinite along  $x$ - and  $y$ -axes, i.e., in the plane of the film-  
substrate interface. Hereafter, we approximate the total po-  
tential at each point inside the capacitor as a sum of all  
potentials due to all charges in the system at that point (ex-  
cluding the particular point itself). Using this superposition  
principle of electrostatic potential due to a charge distribu-  
tion in the space between two electrodes, we can discrete-  
wise approximate the total potential,  $\phi$  at a point  $j$  due to the  
space charges situated at all  $k$  in our system as

$$163 \quad \phi_j = \sum_k \phi_{j,k}. \quad (3)$$

Thus,  $\phi_j$  defines the total potential at a point  $j$  due to all  
charges at points  $k$ . We consider three cases corresponding to  
the following distributions:

- (i) exponentially but asymmetrically decaying charge  
density to zero from interfaces 1 (bottom electrode-  
FE) and 2 (FE-top electrode) toward the interior of the  
film [Fig. 1(a)] along with the induced built-in fields  
due to these distributions given in Fig. 1(b),
- (ii) symmetrical charge at both interfaces decaying to  
zero in the middle of the film [Fig. 1(c)] with the  
corresponding built-in field in Fig. 1(c),
- (iii) random distribution of space charge throughout the  
entire film, and,
- (iv) no space charge as the reference state.

The first and second distributions are chosen to simulate  
interfaces that either have high concentration of traps at the  
FE-electrode interfaces or are due to a Schottky-behavior  
resulting from band bending. The third case corresponds to  
film with high density of charge trapping defects throughout  
the volume. The total number of discrete points in the system  
is 500 and each cell length is taken as 0.4 nm, close to the  
unit cell parameter of prototypical perovskite FEs such as  
barium titanate [BaTiO<sub>3</sub>(BT)] or lead zirconate titanate  
[PbZr<sub>1-x</sub>Ti<sub>x</sub>O<sub>3</sub>(PZT  $x/1-x$ )] with Ti-rich stoichiometries.

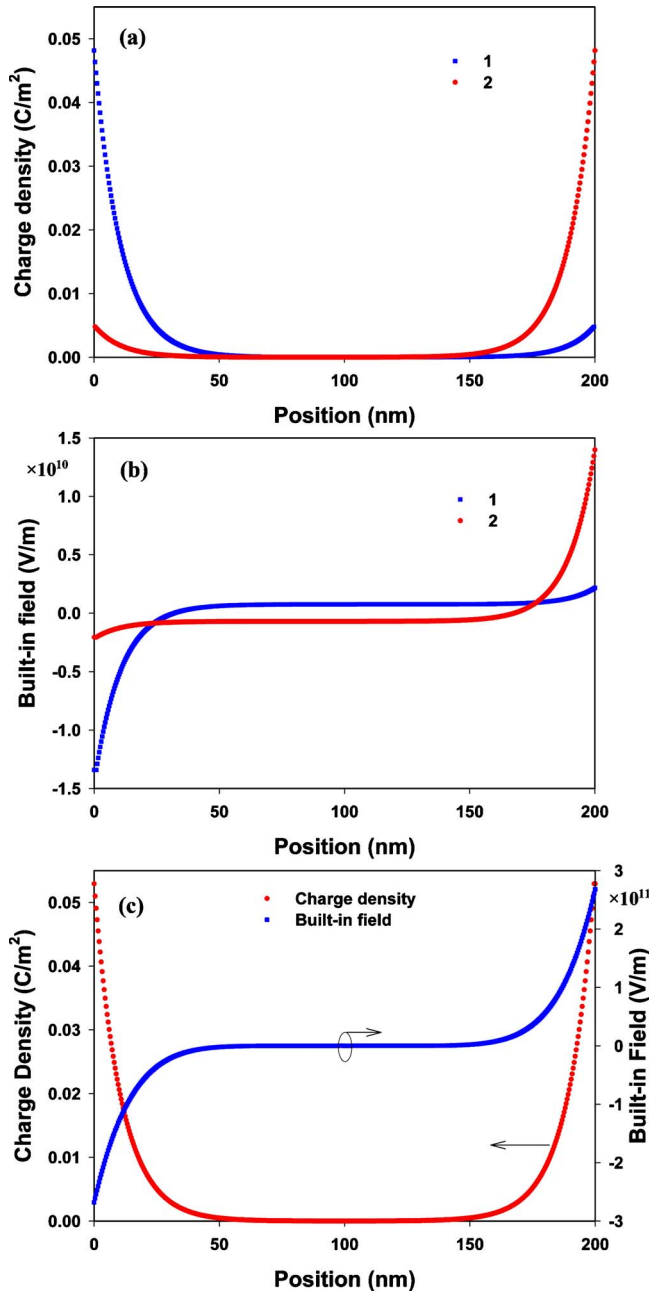


FIG. 1. (Color online) (a) The space charge distribution for the case of asymmetric exponential decay from both film-electrode interfaces toward the interior of the film.  $d_1$  and  $d_2$  correspond to exponential charge injection from the top and bottom electrodes, respectively; (b) the built-in field due to charge distributions  $d_1$  and  $d_2$  in (a); (c) a symmetric distribution of space charges and the corresponding built-in field.

Throughout the current work, we consider that the interaction of the applied potential with the space charge is via a straightforward vectorial addition of the electric fields at each point.

We now proceed with the thermodynamics of the FE film sandwiched between two electrodes and how space charge is introduced to the system energy. The Landau–Ginzburg–Devonshire free energy for an epitaxial monodomain (001) FE film on a (001) cubic substrate can be expressed as

$$F_T = \int_0^L [F_0 + F_P + F_E + F_G - F_{ES}] dz, \quad (5)$$

where  $L$  is the film thickness,  $F_0$  is the energy of the paraelectric state,

$$F_P = \alpha_1(P_1^2 + P_2^2 + P_3^2) + \alpha_{11}(P_1^4 + P_2^4 + P_3^4) + \alpha_{12}(P_1^2 P_2^2 + P_2^2 P_3^2 + P_2^2 P_3^2) + \alpha_{111}(P_1^6 + P_2^6 + P_3^6) + \alpha_{112}[P_1^4(P_2^2 + P_3^2) + P_2^4(P_1^2 + P_3^2) + P_3^4(P_1^2 + P_2^2)] + \alpha_{123}P_1^2 P_2^2 P_3^2, \quad (6)$$

is the energy due to the polarization  $P_i$  ( $i=1, 2, 3$ ) in the FE state, and  $\alpha_i$ ,  $\alpha_{ij}$ , and  $\alpha_{ijk}$  are the dielectric stiffness coefficients.<sup>33</sup>  $F_E$  in Eq. (5) is the internal elastic energy due to epitaxy given by

$$F_E = \frac{1}{S_{11} + S_{12}}(u_m - Q_{12}P_3^2)^2, \quad (7)$$

where  $u_m$  is the in-plane polarization-free misfit strain,  $Q_{12}P_3^2$  is the self-strain in the plane of the film due to polarization along the film thickness, and  $Q_{ij}$  and  $S_{ij}$  are the electrostrictive coefficients and the elastic compliances at constant polarization, respectively, in the contracted notation.

The gradient energy in Eq. (5) is given by

$$F_G = G_{33}\left(\frac{dP_3}{dz}\right)^2 + G_{13}\left(\frac{dP_1}{dz}\right)^2 + G_{23}\left(\frac{dP_2}{dz}\right)^2, \quad (8)$$

where  $G_{ij}$  are the gradient energy coefficients.

The last term entering Eq. (5) is the electrostatic energy. In its most general form, it can be expressed as

$$F_{ES} = \left[ E_{APP} + E(z) - \frac{1}{2}E_D(z) \right] P_3, \quad (9)$$

and the total field  $E_3$  at a position  $j$  due to the electrostatic interactions is given as

$$E_3 = E_{APP} + E(z) - E_D(z). \quad (10)$$

In Eqs. (9) and (10),  $E_{APP}$  is the external applied field,  $E(z)$  is the built-in field due to the space charges attaining its value from Eq. (4), and  $E_D$  is the depolarization field arising due to the polarization variations at the interfaces resulting in bound charges.  $E(z)$  and  $E_D$  are both functions of position and the latter is given as

$$E_D(z) = \frac{1}{\epsilon_0} \left[ P_3 - \frac{1}{L} \int_0^L P_3 dz \right]. \quad (11)$$

188 Once the total built-in potential at each point in the system is  
189 established, the local internal field  $E$  can simply be computed  
190 from the gradient of the potential  $\phi_j$  along the  $z$ -axis via

$$191 \quad E_j = -\nabla \phi_j. \quad (4)$$

192 We should also mention here that the above approach is  
193 for a capacitor whose electrodes are kept at zero potential. In  
194 the presence of an externally applied potential, where experi-  
195 mentally one electrode often attains a particular sign while  
196 the other is kept at ground, the internal total potential due to  
197 the space charge distribution might vary as the boundary  
198 conditions change for the solution of the Poisson's equation.

For thin layers (at the order of a few nanometers) and highly inhomogeneous structures, the gradient energy may have a significant effect on polarization and cannot be neglected. In our calculations, we shall assume that the gradient energy is isotropic, and thus  $G_{33}=G_{13}=G_{23}=G$ . Furthermore, the in-plane biaxial internal stress state with equal orthogonal components due to epitaxy require that  $P_1=P_2$ . Thus we obtain the following Euler–Lagrange relations from the equations of state  $\partial F_T/\partial P_3=0$  and  $\partial F_T/\partial P_1=0$

$$G \frac{d^2 P_3}{dz^2} = 2\alpha_3^m P_3 + 4\alpha_{13}^m P_3 P_1^2 + 4\alpha_{33}^m P_3^3 + 6\alpha_{111} P_3^5 + \alpha_{112}(4P_3 P_1^4 + 8P_3^3 P_1^2) + 2\alpha_{123} P_3 P_1^4 - \left[ E_{APP} + E_B - \frac{1}{\epsilon_0 L} \int_0^L P_3 dz \right], \quad (12)$$

$$G \frac{d^2 P_1}{dz^2} = 2\alpha_1^m P_1 + 2(2\alpha_{11}^m + \alpha_{12}^m) P_1^3 + 2\alpha_{13}^m P_1 P_3^2 + 6\alpha_{111} P_1^5 + 2\alpha_{112}[3P_1^5 + 3P_1^3 P_3^2 + P_1 P_3^4] + 2\alpha_{123} P_1^3 P_3^2, \quad (13)$$

where the  $\alpha_3^m$ ,  $\alpha_{13}^m$ , and  $\alpha_{33}^m$  are the renormalized dielectric stiffness coefficients, modified by the misfit strain, the depolarizing field, and the two-dimensional clamping of the film.<sup>34</sup> We note that the only dielectric stiffness coefficient that is renormalized due to the depolarizing field is  $\alpha_3^m$  and is given by

$$\alpha_3^m = \alpha_1 - u_m \frac{2Q_{12}}{S_{11} + S_{12}} + \frac{1}{\epsilon_0}, \quad (14)$$

as a result of the emergence of the  $P_3^2/\epsilon_0$  term coming from the depolarization field energy [Eqs. (9)–(11)]. The boundary conditions at the interfaces employed for the films are

$$\left[ P_1 + \lambda \frac{dP_1}{dz} \right]_{z=0,L} = 0, \quad (15a)$$

$$\left[ P_3 + \lambda \frac{dP_3}{dz} \right]_{z=0,L} = 0, \quad (15b)$$

and  $\lambda$  is the extrapolation length. Equation (15b) implies that there are no surface fields at the FE-electrode interfaces. Therefore, the only depolarizing field contribution in the system are due to the local variations in  $P_3$  induced by space charges, which are weakly screened by the background dielectric constant. The materials system considered in this study is a 200 nm thick heteroepitaxial (001) PZT 30/70 on a (001) SrTiO<sub>3</sub> (ST) substrate with pseudomorphic top and bottom metallic electrodes. The values of the dielectric stiffness coefficients and other thermodynamic parameters entering the calculations are given in Table I. The equations of state given in Eqs. (12) and (13) have to be solved simultaneously with the boundary conditions given in Eqs. (15a) and (15b). To obtain the polarizations at different space charge and applied fields and different temperatures, we use a Gauss–Seidel iterative scheme where we start with random

TABLE I. Thermodynamic parameters, free energy coefficients, electromechanical, and elastic coefficients of PZT 30/70 used in this study, from Ref. 33.

|   | PZT 30/70         |
|---|-------------------|
| $T_C$ (°C, bulk)  | 440               |
| $\epsilon_0$ ( $10^{-12}$ F/m)                            | 8.85              |
| $C$ (°C)  | $1.5 \times 10^5$ |
| $\alpha_{11}$ ( $10^7$ m <sup>5</sup> /C <sup>2</sup> F)  | 0.6458            |
| $\alpha_{111}$ ( $10^8$ m <sup>9</sup> /C <sup>4</sup> F) | 2.348             |
| $\alpha_{12}$ ( $10^8$ m <sup>5</sup> /C <sup>2</sup> F)  | 5.109             |
| $\alpha_{112}$ ( $10^8$ m <sup>9</sup> /C <sup>4</sup> F) | 10.25             |
| $\alpha_{123}$ ( $10^8$ m <sup>9</sup> /C <sup>4</sup> F) | −5.003            |
| $S_{11}$ ( $10^{-12}$ Pa <sup>−1</sup> )                  | 8.4               |
| $S_{12}$ ( $10^{-12}$ Pa <sup>−1</sup> )                  | −1.7              |
| $S_{44}$ ( $10^{-12}$ Pa <sup>−1</sup> )                  | 9.24              |
| $Q_{11}$ ( $10^{-2}$ m <sup>4</sup> /C <sup>2</sup> )     | 7.887             |
| $Q_{12}$ ( $10^{-2}$ m <sup>4</sup> /C <sup>2</sup> )     | −2.480            |
| $Q_{44}$ ( $10^{-2}$ m <sup>4</sup> /C <sup>2</sup> )     | 6.356             |
| $D_{33}, D_{13}, D_{23}$ ( $10^{-9}$ m <sup>3</sup> /F)   | 5.0               |
| $\lambda$ (m)   | Infinite          |
| $u_m$ at RT   | −0.0166           |

polarization distributions in the system that converges to the real solution after a number of iterations.

The temperature-polarization ( $T$ – $P_3$ ) curves reflect the equilibrium polarization at each temperature interval in the presence and absence of space charge distribution. The quasi-static  $P_3$ – $E_{APP}$  hysteresis curves are at room temperature (RT=25 °C) obtained by applying a triangular field that has a maximum amplitude of  $5 \times 10^8$  V/m and incremental values of  $2.5 \times 10^7$  V/m, adding up to a total of 100 steps. At each field, the polarization as a function of position is computed using the iterative method detailed above. In both the temperature dependence of the polarization and the hysteresis loop computations, the values of polarization obtained for a given state are fed as initial values for the next iterative run, ensuring high convergence precision. The small signal average dielectric constant of the system along  $z$  is found from

$$\epsilon(T, \rho) = \frac{D_3(T, \rho, E_S) - D_3(T, \rho, E_{APP} = 0)}{E_S}, \quad (16)$$

where  $D_3$  is the dielectric displacement of the film along the  $z$ -axis obtained at the end of the numerical iteration for zero field followed by for a small signal field,  $E_S=1$  V/m. The in-plane misfit strain considered in all computations corresponds to a pseudomorphic (001) PZT 30/70 film on a (001) ST substrate (−1.66% at room temperature). During the numerical iteration, although we took into account the possible presence of an in-plane polarization in PZT 30/70, the solution of the in-plane components comes out as zero for the considered strain state. In the  $T$ – $P$  plots, to be able clearly judge the effect of space charge and avoid complications due to thermal strain effects on the PT characteristics, we assumed both the substrate and the FE film have the same thermal expansion coefficients. The reason for this assumption is that while thermal strains as well as stress relaxation due to the formation of interfacial dislocations can easily be

318 incorporated into the current analysis, these might mask  
 319 space charge related changes in the polarization and dielec-  
 320 tric response.

### 321 III. RESULTS AND DISCUSSION

#### 322 A. FE Hysteresis Loops

323 As one of the prominent observations in FE thin films  
 324 compared to their bulk counterparts is the asymmetry in the  
 325  $P-E_{APP}$  ( $P=P_3$ ) hysteresis loops, we first focus on the effect  
 326 of charge distributions at interfaces that decay exponentially  
 327 toward the interior of the film. Such an accumulated charge  
 328 density near interfaces will induce asymmetric potentials in  
 329 the film resulting in internal electric fields that might favor  
 330 an asymmetric variation in  $P(z)$ . An example of the charge  
 331 distribution at interface 1 with a maximum planar density  
 332 amplitude of  $0.05 \text{ C/m}^2$  at interface 1 and  $1/10$ th of this  
 333 value at interface 2 (denoted as distribution 1 or d1), and  
 334 vice versa (distribution 2, d2) are given in Fig. 1(a). The  
 335 built-in fields associated with d1 and d2 are plotted in Fig.  
 336 1(b). The gradient of the potential is steeper toward inter-  
 337 faces, creating the highest internal fields in this region for  
 338 both of the two cases. The maximum amplitude of the charge  
 339 density can be adjusted or a random distribution could also  
 340 be defined. We did so for maximum asymmetric local density  
 341 amplitudes of  $0.05$  and  $0.075 \text{ C/m}^2$  for both d1 and d2.  
 342 Such a spatial density of space charge accumulating on either  
 343 side of the capacitor structure should be expected to pin the  
 344 polarization when the bias field it creates is comparable to  
 345 the thermodynamic coercive field.

346 Assuming perfect electrodes and infinite extrapolation  
 347 length at the interfaces, together with incorporation of the  
 348 small screening contribution from the background dielectric  
 349 constant to the depolarizing field term, we find the spontane-  
 350 ous polarization at zero field and RT the same as the analyti-  
 351 cally computed value ( $\sim 0.7 \text{ C/m}^2$ ,  $T_C \sim 900 \text{ }^\circ\text{C}$ ) for a mon-  
 352 odomain pseudomorphic (001) PZT 30/70 film on (001) ST.  
 353 We note that for a perfect film with perfect electrodes and  
 354 infinite extrapolation length, there is no depolarization as the  
 355 polarization is homogeneous throughout the thickness of the  
 356 film. The  $P-E$  hysteresis are computed for the charge den-  
 357 sity distributions given in Fig. 1 with the form of d1 and d2  
 358 for maximum planar densities of  $0.05 \text{ C/m}^2$  and  
 359  $0.075 \text{ C/m}^2$  displayed in Figs. 2(a) and 2(b), respectively.  
 360 Changing the maximum local planar density amplitude to  
 361  $0.075 \text{ C/m}^2$  does not change the form of the distribution but  
 362 only the local values that are used to plot Fig. 1(b). As shown  
 363 in Fig. 2, the shift of the hysteresis loops depends on the way  
 364 space charge is distributed as well as its local concentration  
 365 in the film. We note that we only exchange the amplitudes of  
 366 planar space charges to obtain d1 and d2 but not the sign of  
 367 charge. Furthermore, another important finding is that the  
 368  $P-E_{APP}$  loops under asymmetrically distributed high space  
 369 charge densities near the interfaces (such as in the case of  
 370  $0.075 \text{ C/m}^2$  local planar density) can be shifted along the  
 371 applied field axis such that  $E_{C^-}, E_{C^+} > 0$  or  $E_{C^-}, E_{C^+} < 0$  com-  
 372 pared to charge-free films for which  $|E_{C^-}| = E_{C^+}$  and  $\Delta E$   
 373  $= E_{C^+} - |E_{C^-}| = 0$  [also shown in Figs. 2(a)–2(c) as a refer-  
 374 ence]. Similar behavior was discussed in Ref. 2 where irra-

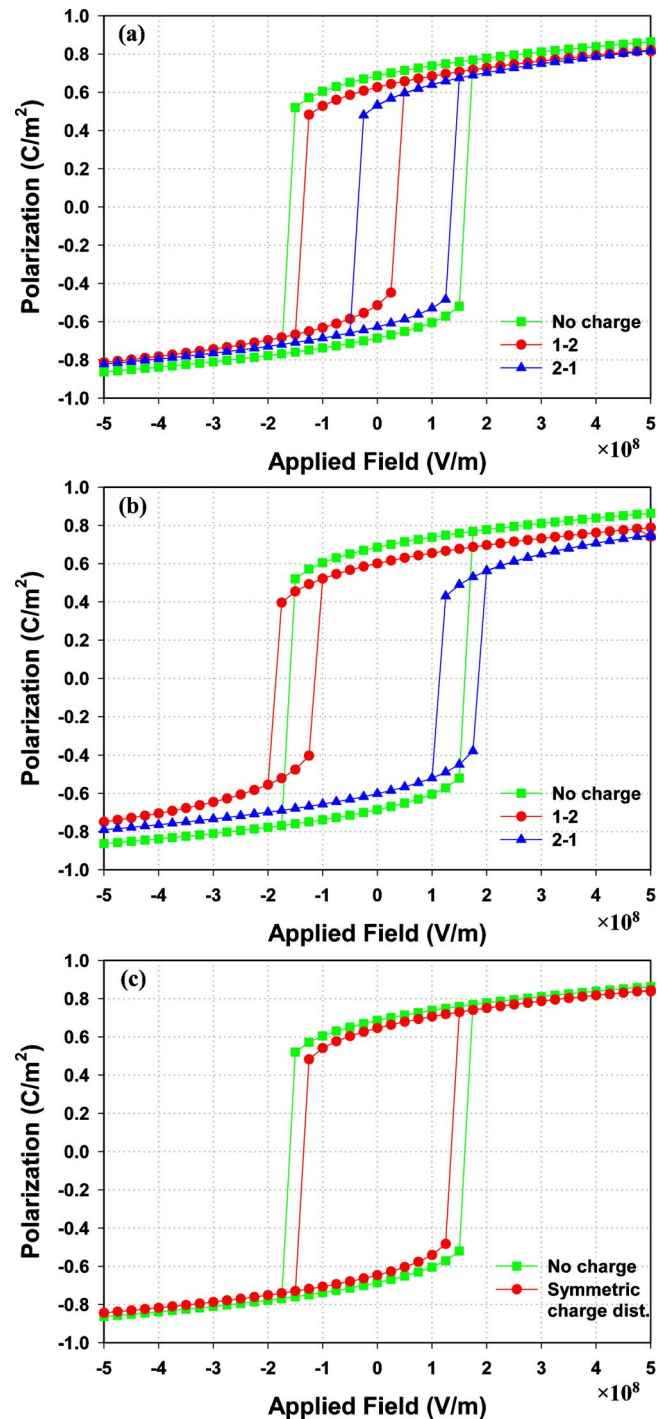


FIG. 2. (Color online) The displacement of the polarization-applied electric field hysteresis curves due to asymmetrically exponential decay of space charge distributions with a maximum amplitude of (a)  $0.05 \text{ C/m}^2$  and (b)  $0.075 \text{ C/m}^2$  with charge distribution d1 and d2, respectively; and (c) fully symmetric charge distribution with  $0.05 \text{ C/m}^2$  at each interface. The hysteresis curves outlined by solid squares in (a), (b), and (c) correspond to films with no space charges.

diated triglycine sulfate samples were shown to display 375  
 strongly shifted or deformed hysteresis response. One must 376  
 note here that a fixed space charge density is considered in 377  
 this study within the thermodynamic limit. Changes in tem- 378  
 perature and band bending during polarization switching of 379  
 the electrode-FE-electrode system could make the space 380  
 charge density a dynamic parameter where it becomes a 381  
 function of the applied field. 382

383 To elucidate the formation of space charges even in  
 384 nearly defect-free films where behavior similar to that in Fig.  
 385 2 might be observed, we provide the following example.  
 386 Epitaxial growth of FE films on metallized single-crystal  
 387 substrates is usually carried out at relatively high tempera-  
 388 tures (typically in the range of 500–800 °C) in controlled  
 389 oxygen atmospheres followed by cooling. The sample is then  
 390 taken out of the chamber for the placement of a mask to  
 391 enable the growth of top electrodes, typically achieved via  
 392 rf-sputtering or thermal evaporation. The diameter of the top  
 393 electrodes may vary from a few hundred nanometers to a few  
 394 tens of microns. This processing sequence may actually pro-  
 395 mote an asymmetric charge injection at the two FE-electrode  
 396 interfaces just because a different deposition method at a  
 397 different temperature was used to grow the bottom electrode,  
 398 the FE film, and the top electrode. Moreover, the formation  
 399 of asymmetrical space charges may result from the termina-  
 400 tion of different atomic planes of the FE film. One must also  
 401 note that an average negative bias due to asymmetric surface  
 402 effects or near-interface charges displaces the hysteresis loop  
 403 toward the positive  $E_{APP}$ -axis and vice versa.

404 In order to provide a complimentary view of the effect of  
 405 distribution of the space charges throughout the film, we give  
 406 in Fig. 2(c) the hysteresis loop of a FE film when there are  
 407 equal concentrations of fixed space charges that decay expo-  
 408 nentially from both interfaces. Due to the symmetry of the  
 409 internal electric field distribution in the film, there is no dis-  
 410 placement of the hysteresis loops but there is a considerable  
 411 reduction in the coercive field, consistent with our recent  
 412 findings.<sup>17</sup> This is due to the depolarization field that arises  
 413 from the inhomogeneous variation in the polarization along  
 414 the film thickness as well as the commensurate gradient en-  
 415 ergy. As such, the phase transition temperature  $T_C$  is reduced.  
 416 The behavior of the total polarization as a function of the  
 417 temperature is discussed in Sec. III B.

#### 418 B. Phase transition temperature and dielectric 419 properties

420 Using the methodology described in Sec. III A, we cal-  
 421 culated the total polarization and the dielectric response of  
 422 the FE film as a function of the temperature for a perfect film  
 423 with no space charges and a film with asymmetric distribu-  
 424 tion of space charge densities. Figure 3 plots the temperature  
 425 dependence of the polarization and the dielectric constant of  
 426 the (001) PZT 30/70 film on (001) ST with no space charges  
 427 and a space charge distribution d1 with a maximum ampli-  
 428 tude of 0.05 C/m<sup>2</sup>. For the case for  $\rho=0$ , the spontaneous  
 429 polarization in the film vanishes above  $T_C$ , and, as expected,  
 430 there is a  $\lambda$ -type anomaly in the dielectric response at  $T_C$ .  
 431 However, if there is an inhomogeneous distribution of the  
 432 space charges, the phase transformation is “smeared” over a  
 433 temperature interval rather than a singular transition point as  
 434 it is the case for  $\rho=0$ . Furthermore, there is also a significant  
 435 reduction in the dielectric properties near  $T_C$  for films with  
 436 asymmetric space charge distributions (Fig. 3). For asym-  
 437 metric variations in the space charge, there is a nearly  
 438 temperature-insensitive polarization above the effective  $T_C$   
 439 that is essentially the built-in polarization due to the space  
 440 charges. For higher values of the space charge density, the

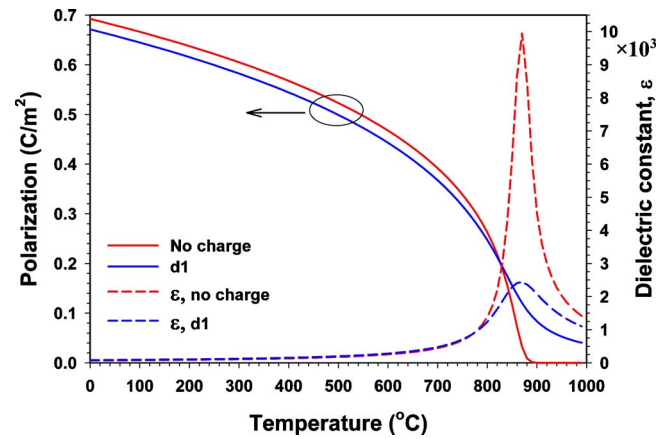


FIG. 3. (Color online) Total polarization and the dielectric constant as a function of temperature in the absence of space charges and with space charges (d1, with a maximum of 0.05 C/m<sup>2</sup>).

441 transition becomes a very gradual one, almost a linear varia-  
 442 tion in polarization with temperature with no apparent phase  
 443 transformation temperature. While there is a small reduction  
 444 in the polarization values and  $T_C$ , the latter is considerably  
 445 more pronounced for a system with a random distribution of  
 446 space charges which will be discussed next. We note here the  
 447 space charge concentrations may not necessarily remain const-  
 448 ant as it is assumed in our analysis at temperatures near  $T_C$   
 449 and could be expected to be reduced (or entirely neutralized)  
 450 via thermally excited carriers. Such a process may thus re-  
 451 duce (or completely eliminate) the built-in fields at tempera-  
 452 tures near the  $T_C$  of strained PZT 30/70.

453 In Fig. 4, we provide the temperature dependence of the  
 454 total polarization and the dielectric response for the case of a  
 455 random space charge variation throughout the film thickness.  
 456 Such a distribution introduces almost a linearly varying  
 457 built-in field that changes sign near the middle of the film.  
 458 This field results in a drastic reduction in  $T_C$  while there is a  
 459 sharper dielectric anomaly at  $T_C$  compared to the conditions  
 460 corresponding to asymmetric distribution of space charges  
 461 discussed in connection with Fig. 3. We also note that the  
 462 dielectric constant of the film with random variation in high  
 463 density space charges at RT given in Fig. 4 is higher than the

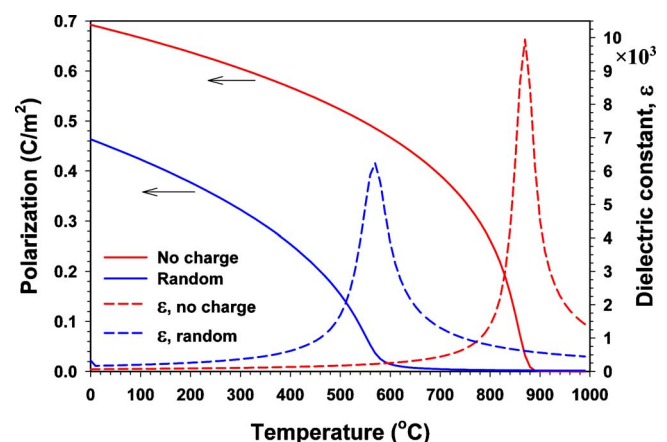


FIG. 4. (Color online) Total polarization and the dielectric constant as a function of temperature in the absence of space charges and with randomly distributed space charges with a maximum planar density of 0.05 C/m<sup>2</sup>.

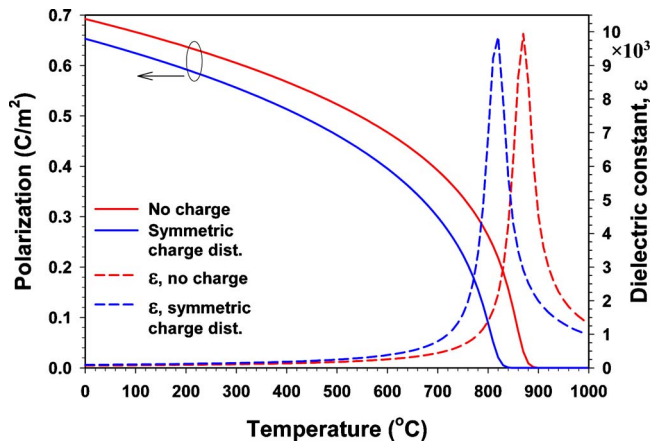


FIG. 5. (Color online) Total polarization and the dielectric constant as a function of temperature in the absence of space charges and with a completely symmetrical continuous distribution of space charge at both interfaces decaying exponentially toward the interior of the film.

same charge density distribution whose potential will be- 504  
 come steeper (for zero potential at the electrodes), creating 505  
 larger internal built-in fields can be expected to render a 506  
 stronger  $P$  pinning highly probable. The strongly inhomoge- 507  
 neous fields acting at distances at the order of a few nanom- 508  
 eters due to space charge lead to greater spatial variation in 509  
 the polarization and hence yield higher depolarizing fields, 510  
 resulting in a larger reduction in  $T_C$ , similar to the finite size 511  
 effect.<sup>35</sup> This decrease should certainly be much more dra- 512  
 matic for highly asymmetrical distributions of space charges. 513  
 We note that even if the switchable FE polarization disap- 514  
 pears at temperatures above  $T_C$ , the space charge induced 515  
 temperature-independent polarization will remain. In addi- 516  
 tion, a stronger smearing of the transition temperature could 517  
 also be expected as already discussed in Ref. 36. This is, of 518  
 course, possible for materials with low  $T_C$  wherein thermally 519  
 excited neutralization mechanisms of space charges will not 520  
 be significant. For films with high  $T_C$ , thermally excited car- 521  
 riers from the traps could take effect in neutralization of the 522  
 space charges at elevated temperatures, reducing the smear- 523  
 ing effects. 524

#### IV. CONCLUSIONS 525

Using a nonlinear thermodynamic model coupled with 526  
 an electrostatic analysis, we have investigated the effects of a 527  
 continuous distribution of planar space charges along the 528  
 film thickness on the phase transition characteristics, hysteresis 529  
 response, and dielectric properties of epitaxial (001) 530  
 PZT 30/70 films between metallic electrodes on (001) STO 531  
 substrates. It is shown that asymmetrically distributed space 532  
 charges result in displacements in the  $P$ - $E_{APP}$  hysteresis 533  
 curves along the applied field axis and may even give rise to 534  
 coercive fields  $E_{C^-}, E_{C^+} > 0$  or  $E_{C^-}, E_{C^+} < 0$  compared to 535  
 charge-free films for which  $|E_{C^-}| = E_{C^+}$  and  $\Delta E = E_{C^+} - |E_{C^-}|$  536  
 $= 0$ . These trapped charges may significantly smear out the 537  
 FE phase transition and reduce  $T_C$ . If the space charges are 538  
 symmetrically distributed, the FE hysteresis loops shrink 539  
 along both the polarization and the applied field axes but 540  
 remain centered at the origin. For relatively high charge den- 541  
 sities, we find that a monodomain FE film cannot be 542  
 switched from one polarization state to another under typical 543  
 cyclic (e.g., completely reversed sinusoidal) electrical bias 544  
 with an amplitude  $2 \cdot E_{APP}$ . A polydomain structure may form 545  
 in FE films to minimize internal depolarizing fields originat- 546  
 ing from local variations in the polarization. However, the 547  
 strong internal bias due to an asymmetric charge distribution 548  
 may preclude the generation of electrical domains. The 549  
 analysis presented herein is in the limit of thermodynamics 550  
 and future time-dependent studies should focus on nucleation 551  
 and growth kinetics of domains during switching in the pres- 552  
 ence of a spatial space charge distribution. In such dynamic 553  
 models, the trapping and emission rates of carriers have to be 554  
 considered as well. 555

#### ACKNOWLEDGMENTS 556

I. B. M. acknowledges the hardware and software sup- 557  
 port of Sabanci University. The work at the University of 558  
 Connecticut was funded by the U.S. Army Research Office 559

464 films with  $\rho=0$  because of the significant reduction in  $T_C$ , in 465  
 agreement with the findings of Ref. 3. Above the effective 466  
 $T_C$ , there is nearly no net built-in polarization due to the 467  
 opposite but nearly equal polarization profile in the two 468  
 halves of the film with respect to the middle of the film at 469  
 zero field.

470 Figure 5 plots the temperature dependence of the total 471  
 polarization and the dielectric response in the case of a sym- 472  
 metrical charge distribution given in Fig. 1(c). A symmetrical 473  
 variation in the planar space charge concentration removes 474  
 any net internal bias in the system and the dielectric anomaly 475  
 at  $T_C$  is nearly the same as that of the perfect film with no net 476  
 built-in polarization except a slight reduction in  $T_C$  and  $P$ . 477  
 From Fig. 5, one can observe a near zero built-in polarization 478  
 above  $T_C$  as a consequence of the nearly equal internal field 479  
 due to space charges in the two halves of the film. Due to the 480  
 absence of a net bias field, the induced polarization due to 481  
 space charges is weak and there is no smearing of the dielec- 482  
 tric response at  $T_C$ . The fields due to space charges are 483  
 mostly confined to the near-interface regions with exactly 484  
 equal but opposite signs, giving rise to a symmetrical polar- 485  
 ization variation below  $T_C$ . It should also be expected that 486  
 the depolarizing field term has a more pronounced effect 487  
 near the interfaces where the polarization changes drastically 488  
 over relatively short distances. Thus, the small reduction in 489  
 the remnant polarization at all temperatures below  $T_C$  com- 490  
 pared to the charge-free film is mostly due to the inhomoge- 491  
 neous variation in the local polarization near the film- 492  
 electrode interfaces. The changes in the polarization near the 493  
 electrode interfaces also increases the gradient energy. 494  
 Therefore, the combination of both the depolarization and 495  
 the gradient energy act to slightly reduce  $T_C$ .

496 Overall, the gradual nature of the transition in the pres- 497  
 ence of asymmetric space charge dramatically reduces the 498  
 dielectric anomaly that is a characteristic of the charge-free 499  
 film in addition to a considerable drop in  $T_C$ . One must note 500  
 that polarization, if computed for the FE phase with high 501  
 space charge densities, is actually the susceptibility of the 502  
 “pinned” or imprinted polarization concurrent with an asym- 503  
 metrically distributed space charge. For thinner films, the

- 560 through Grant Nos. W911NF-05-1-0528 and W911NF-08-C-  
561 0124.
- 562 <sup>1</sup>S. Triebwasser, *Phys. Rev.* **118**, 100 (1960).
- 563 <sup>2</sup>A. P. Levanyuk and A. S. Sigov, in *Defects and Structural Phase Transitions*,  
564 *Ferroelectricity and Related Phenomena*, edited by W. Taylor, Vol. 6  
565 (Gordon and Breach Science, ■, 1988).
- AQ: 566 <sup>3</sup>A. M. Bratkovsky and A. P. Levanyuk, *Phys. Rev. B* **61**, 15042 (2000).
- #2 567 <sup>4</sup>B. Zhang, H.-S. Kwok, and H.-C. Huang, *J. Appl. Phys.* **98**, 123103  
AQ: 568 (2005).
- #3 569 <sup>5</sup>Y. Xiao, V. B. Shenoy, and K. Bhattacharya, *Phys. Rev. Lett.* **95**, 247603  
570 (2005).
- 571 <sup>6</sup>A. K. Tagantsev and G. Gerra, *J. Appl. Phys.* **100**, 051607 (2006).
- 572 <sup>7</sup>L. Pintilie, *Phys. Rev. B* **75**, 224113 (2007).
- 573 <sup>8</sup>L. Pintilie, I. Vrejoiu, M. Alexe, and D. Hesse, *J. Appl. Phys.* **104**, 114101  
574 (2008).
- 575 <sup>9</sup>E. G. Lee, D. J. Wouters, G. Willems, and H. E. Maes, *Appl. Phys. Lett.*  
576 **69**, 1223 (1996).
- 577 <sup>10</sup>G. Le Rhun, R. Bouregba, and G. Poullain, *J. Appl. Phys.* **96**, 5712 (2004).
- 578 <sup>11</sup>See, for example, D. Balzar, P. A. Ramakrishnan, and A. M. Hermann,  
579 *Phys. Rev. B* **70**, 092103 (2004); I. B. Misirlioglu, S. P. Alpay, M. Aindow,  
580 and V. Nagarajan, *Appl. Phys. Lett.* **88**, 102906 (2006).
- 581 <sup>12</sup>M. Alexe, *Appl. Phys. Lett.* **72**, 2283 (1998).
- 582 <sup>13</sup>D. O'Neill, R. M. Bowman, and J. M. Gregg, *Appl. Phys. Lett.* **77**, 1520  
583 (2000).
- 584 <sup>14</sup>J. Mcaneney, L. J. Sinnamon, A. Lookman, R. M. Bowman, and J. M.  
585 Gregg, *Integr. Ferroelectr.* **60**, 79 (2004).
- 586 <sup>15</sup>D. Fu, K. Suzuki, K. Kato, and H. Suzuki, *Appl. Phys. A: Mater. Sci.*  
587 *Process.* **80**, 1067 (2005).
- 588 <sup>16</sup>P. Zubko, D. J. Jung, and J. F. Scott, *J. Appl. Phys.* **100**, 114112 (2006).
- 589 <sup>17</sup>M. B. Okatan, J. V. Mantese, and S. P. Alpay, *Phys. Rev. B* **79**, 174113  
590 (2009); *Acta Mater.* **58**, 39 (2010).
- 591 <sup>18</sup>L. Courtade, C. Muller, G. Andreoli, C. Turquat, L. Goux, and D. J. Wouters, *Appl. Phys. Lett.* **89**, 113501 (2006). **592**
- <sup>19</sup>L. Goux, Z. Xu, V. Paraschiv, J. G. Lisoni, D. Maes, L. Haspeslagh, G. Groeseneken, and D. J. Wouters, *Solid-State Electron.* **50**, 1227 (2006). **593**
- <sup>20</sup>W. B. Wu, K. H. Wong, C. L. Mak, C. L. Choy, and Y. H. Zhang, *J. Vac. Sci. Technol. A* **18**, 2412 (2000). **594**
- <sup>21</sup>W. B. Wu, K. H. Wong, and C. L. Choy, *Appl. Phys. Lett.* **85**, 5013 (2004). **595**
- <sup>22</sup>A. Z. Simoes, C. S. Riccardi, A. H. M. Gonzalez, A. Ries, E. Longo, and J. A. Varela, *Mater. Res. Bull.* **42**, 967 (2007). **596**
- <sup>23</sup>L. Feigl, E. Pippel, L. Pintilie, M. Alexe, and D. Hesse, *J. Appl. Phys.* **105**, 126103 (2009). **597**
- <sup>24</sup>A. K. Tagantsev, I. Stolichnov, N. Setter, and J. S. Cross, *J. Appl. Phys.* **96**, 6616 (2004). **598**
- <sup>25</sup>A. N. Morozovska and E. A. Eliseev, *J. Phys. Condens. Matter* **16**, 8937 (2004). **599**
- <sup>26</sup>Y. Zhou, H. K. Chan, C. H. Lam, and F. G. Shin, *J. Appl. Phys.* **98**, 024111 (2005). **600**
- <sup>27</sup>H. X. Cao, V. C. Lo, and Z. Y. Li, *Solid State Commun.* **138**, 404 (2006). **601**
- <sup>28</sup>I. B. Misirlioglu, M. Alexe, L. Pintilie, and D. Hesse, *Appl. Phys. Lett.* **91**, 022911 (2007). **602**
- <sup>29</sup>O. Dahl, J. K. Grepstad, and T. Tybell, *J. Appl. Phys.* **106**, 084104 (2009). **603**
- <sup>30</sup>X. J. Zheng, W. Yin, T. Zhang, Q. Chen, M. H. Tang, and J. Sun, *Phys. Status Solidi (RRL)* **3**, 251 (2009). **604**
- <sup>31</sup>M. B. Okatan and S. P. Alpay, *Appl. Phys. Lett.* **95**, 092902 (2009). **605**
- <sup>32</sup>A. K. Tagantsev, *Ferroelectrics* **375**, 19 (2008). **606**
- <sup>33</sup>M. J. Haun, Z. Q. Zhuang, E. Furman, S. J. Jang, and L. E. Cross, *Ferroelectrics* **99**, 45 (1989). **607**
- <sup>34</sup>N. A. Pertsev, A. G. Zembilgotov, and A. K. Tagantsev, *Phys. Rev. Lett.* **80**, 1988 (1998). **608**
- <sup>35</sup>A. M. Bratkovsky and A. P. Levanyuk, *Phys. Rev. Lett.* **94**, 107601 (2005). **609**
- <sup>36</sup>See, for example, E. K. Akdogan and A. Safari, *J. Appl. Phys.* **101**, 064114 (2007); **101**, 064115 (2007). **610**
- 611**
- 612**
- 613**
- 614**
- 615**
- 616**
- 617**
- 618**
- 619**
- 620**
- 621**
- 622**
- 623**
- 624**

**AUTHOR QUERIES — 106013JAP**

- #1 Au: Please verify the renumbering of references from Ref. 15 to Ref. 23 and from Ref. 35 to Ref. 36, as they were out of order.
- #2 Au: Please provide publisher location in Ref. 2.
- #3 Au: Please verify the change made in author names in Ref. 4.